

## Galactic chemical evolution

M. Mollá<sup>1</sup>, O. Cavichia<sup>2</sup>, R. da Costa<sup>3</sup>, B.K. Gibson<sup>4</sup>, and A.I. Díaz<sup>5,6</sup>

<sup>1</sup> Departamento de Investigación Básica, CIEMAT, Avda. Complutense 40, E-28040 Madrid. (Spain)

<sup>2</sup> Instituto de Física e Química, Universidade Federal de Itajubá, Av. BPS, 1303, 37500-903, Itajubá-MG, Brazil

<sup>3</sup> Instituto de Astronomia, Geofísica e Ciências Atmosféricas, Universidade de São Paulo, 05508-900, São Paulo-SP, Brazil

<sup>4</sup> E.A Milne Centre for Astrophysics, University of Hull, HU6 7RX, United Kingdom

<sup>5</sup> Universidad Autónoma de Madrid, 28049, Madrid, Spain

<sup>6</sup> Astro-UAM, Unidad Asociada CSIC, Universidad Autónoma de Madrid, 28049, Madrid, Spain

### Abstract

We analyze the evolution of oxygen abundance radial gradients resulting from our chemical evolution models calculated with different prescriptions for the star formation rate (SFR) and for the gas infall rate, in order to assess their respective roles in shaping gradients. We also compare with cosmological simulations and confront all with recent observational datasets, in particular with abundances inferred from planetary nebulae. We demonstrate the critical importance in isolating the specific radial range over which a gradient is measured, in order for their temporal evolution to be useful indicators of disk growth with redshift.

### 1 Introduction

Chemical elements appear in the Universe as a consequence of three production scenarios: 1) Big Bang Nucleosynthesis; 2) Fragmentation processes (Cosmic Rays); and 3) Stellar Nucleosynthesis. H disappears at the same time that metals (elements heavier than He) increase their abundances. Elements are created, eventually ejected and diluted by the interstellar medium, and ultimately incorporated into successive generations of stars. If the process of star formation occurs rapidly, then the increase of the elemental abundances is also rapid; if it is slow, the abundances also increase slowly. In this way, abundance patterns give clues regarding star formation: when, how, and with which rate, stars form. Galactic Chemical

Evolution (GCE) models try to explain how and when the elements appear based upon some hypothesis [10, 61]. In the process of understanding the creation and evolution of the elements, we might compare model predictions with data and deduce the evolutionary histories of galaxies.

One of the best known features of spiral galaxies is the existence of a radial gradient of abundances in their disks [23]. This gradient was first observed in the Milky Way Galaxy (MWG) and then in other external galaxies [59, 42, 66], and it is now well characterized in our local Universe [57]. The radial gradient was interpreted as due to differences in the star formation rate or the gas infall rate along the disk, although other reasons are also possible –see [22] for a detailed review–. In order to understand the role of the involved processes, numerical chemical evolution models were early developed [33, 34, 14, 62, 41, 15, 16]. Most of these models were able to reproduce the present state of our Galaxy, however not all of them predict the same evolution with time. For example, models from [14, 43] predict an initially flat radial distribution, which then steepens with time. Conversely, models by [15, 16] possess a steep initial radial abundance gradient which flattens with time. The first scenario is the consequence of the existence of the disk before starting the evolution (i.e., initial conditions), combined with an infall of primordial gas which dilutes the metal enrichment of the disk, preferentially in the outer regions. In the second scenario, however, the infall of gas forms out the disk and, furthermore, it contributes to the metal budget because the infalling gas is not primordial: there is also star formation in the halo before the gas falls onto the disk. Therefore, it seems that the radial gradient of abundances, observed in spirals is dependent upon the scenario of formation and evolution of the disk –see [63] and references therein. In fact, as [30] explained, the radial gradient may be only modified by inflows or outflows of gas, and, besides the possible variations of the initial mass function (IMF) or stellar yields along the galactocentric radius, the only way to change a radial gradient of abundances is to have a star formation rate (SFR) or an infall rate changing with galactocentric radius. Most of models able to reproduce the present state of the solar neighborhood and the Galactic disk as a whole follow one of two trends: a) the gradient is steep, and then it flattens with time [16, 50, 44, 49, 25], or, b) it is flat initially and it then steepens with time [62, 43, 8]. Besides this question of the scenario for each chemical evolution model, radial flows of gas or stellar migration may also modify, flattening, the radial distributions of abundances for stars of different ages –see [32] for a review about this subject.

From an observational perspective, the question of appropriate datasets against which to compare has been debated vigorously. In [44] we compared the chemical evolution results with two types of observational data: planetary nebulae (PNe) of different masses (that is, different ages) to oxygen abundance radial distributions at different times, and open and globular clusters, to estimate the global metallicity in objects of different ages. The problem with PNe is that to estimate their galactocentric distances and their stellar masses (and, therefore, their ages) is a process with large uncertainties. The open cluster age determination, in turn, is not an easy task, too, although the error bars are smaller in this case. However the box enclosing the data corresponding to these objects basically falls in the same region of the young stars in a plot of  $[\text{Fe}/\text{H}]$  vs radius. In the end, the most accurate data are those of globular clusters, and based mainly on their metallicities, we reached the conclusion

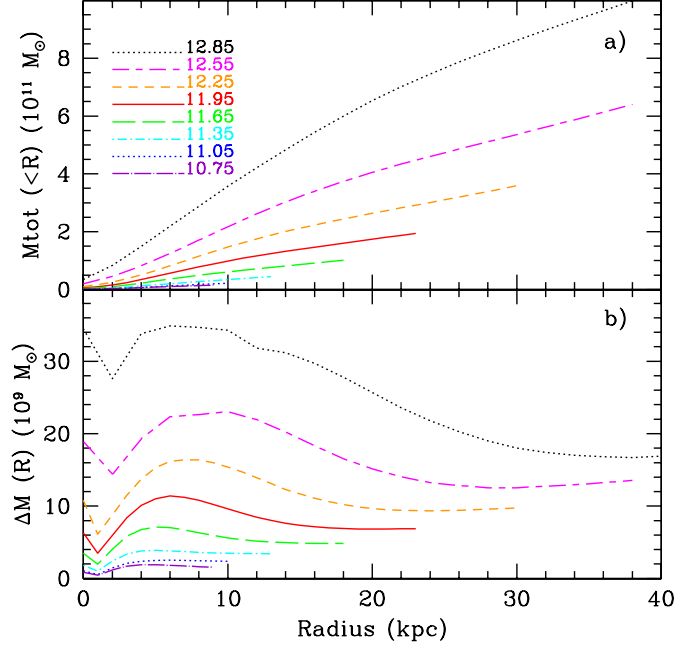


Figure 1: Radial distributions of: a) the total mass; and b) the mass enclosed in each radial region. Different lines correspond to different virial mass values, as labelled. Taken from [47].

that our models with a flattening of the radial gradient of abundances were good enough to reproduce the observational data. This situation has changed, however, in the light of the new observational results of stellar metallicities and of the PNe determinations of age and distance, as we will show later.

We, therefore, think that it is time to revise this question of the evolution of the radial gradient of abundances. To do so, we have generated a new suite of chemical evolution models for which we have revised all the necessary inputs for our code. Here, we will analyze the results corresponding to a Milky Way Galaxy (MWG) like model.

## 2 Chemical Evolution Models

In a chemical evolution model, a scenario is assumed in which there is a given mass of gas in a certain geometric region. This mass is converted to stars by following an assumed star formation law. A mass ejection rate appears as a consequence of the death of stars. Often, some hypothesis concerning gas infall and outflows are included. The ejected mass depends, therefore, on the remnant of each stellar mass, on the mean-lifetimes of stars and on the IMF employed. This suite of models, based on [15, 16], are an update of those from [45], hereinafter MD05. We start with a mass in a proto-halo which is calculated from [55].

We have computed 16 radial distributions within a range of virial masses [ $5 \times 10^{10} - 10^{13}$ ] $M_{\odot}$ , which implies maximum rotation velocities in the range [42 – 320] km s<sup>-1</sup> and leads to disks with total masses in the range [ $1.25 \times 10^8 - 5.3 \times 10^{11}$ ] $M_{\odot}$ . We show in Fig. 1 the radial distributions we have obtained for various virial masses, as labelled.

Shaping the predicted radial abundance patterns are also the: 1) stellar yields (with the corresponding mean-lifetimes of stars) and the IMF; 2) infall rate of gas over the disk, and 3) star formation law, as outlined next.

### 2.1 Stellar Yields

We have divided, as usual, the stellar masses into two ranges corresponding to low- and intermediate-mass stars ( $m < 8M_{\odot}$ ), and massive stars ( $m > 8M_{\odot}$ ). The first eject mainly He<sup>4</sup>, C<sup>12,13</sup> and N<sup>14,15</sup>; a small amount of O can be generated in some yield prescriptions, as well as various s-process isotopes. Massive stars, in turn, produce C, O, and all the so-called  $\alpha$ -elements, up to Fe. The literature of stellar yield generation is a rich one, with various works differing from one another due to the intrinsically different input physics to the underlying stellar models.

Furthermore, it is necessary to deconvolve these stellar yields with the IMF. Again, there are in the literature a certain number of different expressions to define this IMF. Therefore, we have addressed this question in a work described in [46]. There we have computed a chemical evolution model for MWG by using 6 different stellar yields for massive stars, 4 different yields sets for low and intermediate mass stars, and 6 different IMFs. Analyzing these 144 permutations and comparing their results with the observational data for our Galaxy disk, we determined which combinations are most valid in reproducing the data. Following these results, the different IMF + stellar yields combinations produce basically the same radial distributions for gas (diffuse and molecular), and stellar + star formation surface densities, as shown in Fig. 2. The corresponding radial distributions for the elemental abundances of C, N and O, as show in Fig.3, left panel, are very different in their absolute values, with some far from the observational data, while others lie closer to the data. They do, however, show a similar slope for these radial distributions, suggesting that the selection of one or other combination is not particularly useful in modifying the radial abundance *gradient*. In any case, there only 8 combinations IMF + stellar yields able to reproduce the MWG data with a high probability ( $P > 97\%$ ). We use from here the yield combination given by [18, 19] and [35, 9], with the IMF of [31], which provides a good match to the data, as we show in Fig.3,

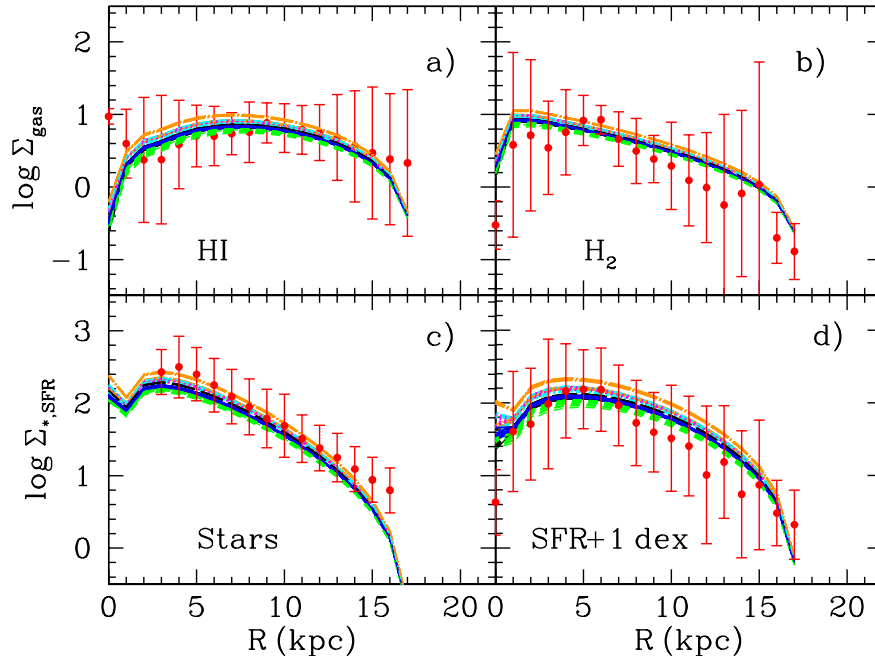


Figure 2: Radial distributions of surface density of: a) diffuse gas, HI; b) molecular gas, H<sub>2</sub>; c) stars and d) SFR. Different lines correspond to different IMF + stellar yields combinations. Dots with error bars are the data for MWG. Taken from [46].

right panel. See more details in [46].

## 2.2 Infall rate

In our scenario, the gas initially in the proto-halo falls to the equatorial plane where the disk forms. In our old MD05 models, we assumed that this infall rate depends on the total mass of each galaxy,  $M$ , through a collapse time-scale  $\tau$ , defined by the expression  $\tau \propto M^{-1/2}$ , from [17]. Moreover, within the disk, and following the same idea as other authors, we had assumed that  $\tau$  has a radial dependence, being shorter in the inner regions of the disk and longer in the outer ones. In fact, we used an exponential function to compute this time scale, at variance with other models where a linear relationship with radius was used. Now, we profit from the new knowledge about the relationship between the halo mass and the corresponding mass of the associated disks to estimate which must be the infall rate from the halo to obtain the correct disk. By using the equation from [58]:

$$M_{\text{star}} [M_{\odot}] = 2.3 \times 10^{10} \frac{(M_{\text{vir}}/3.10^{11} M_{\odot})^{3.1}}{1 + (M_{\text{vir}}/3.10^{11} M_{\odot})^{2.2}}, \quad (1)$$

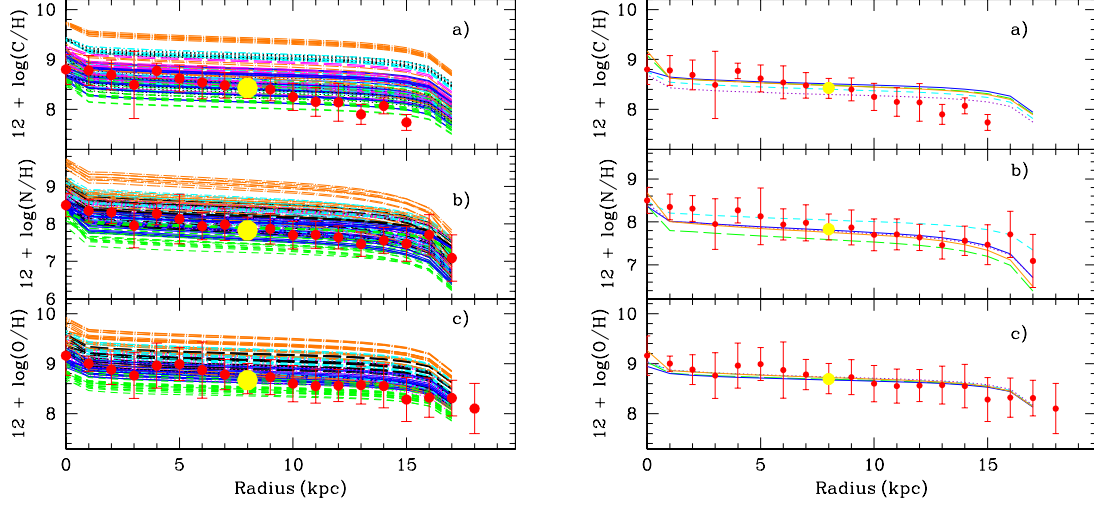


Figure 3: Radial distributions of C, N and O elemental abundances for: a) models with 144 IMF + stellar yield combinations; b) the models selected as the best. Different lines correspond to different IMF + stellar yields combinations. Dots with error bars are the data for MWG as taken from the compilation in [46]. The yellow large dot in each panel is the solar abundance for the corresponding elements. Taken from [46].

it is possible to determine the appropriate final disk mass. From this expression and using the rotation curves and equations from [55], we obtain the radial distributions of mass in the proto-halo and in the disk in each geometrical region at a given galactocentric distance; this is defined by a cylinder, as given in Fig.1. From these masses we obtain the collapse time in each radius  $R$  as:

$$\tau(R) = -\frac{13.2}{\ln\left(1 - \frac{\Delta M_D(R)}{\Delta M_{\text{tot}}(R)}\right)} \text{ [Gyr]} \quad (2)$$

The collapse time scale coming from this expression for a MWG-like model is smoother than the old exponential function used in MD05. The resulting infall rates produced by this collapse timescale are thus different than before: they show a smooth evolution for disks and stronger for bulges. The infall rates for different mass disks show variations only in the absolute values, with a very similar behavior for all galactic masses. The infall rate is very low in the outer regions of disk, and maintains that with redshift. This implies that the SFR is also low for all times. A sharp break in the disk is associated with the dramatic decline in star formation at a given radius.

When we compare these results with the ones coming from cosmological simulations we see that our older models possessed stronger evolution with time, appearing more similar to simulations associated with spheroids/early-types; our newer models are more akin to simulations of late-type disks of the correct size and mass, as shown in Figs. 3 and 6 of [47].

### 2.3 Star formation law

The last of our ingredients refers to the SFR law. In the halo, we assume a Schmidt law to form stars with an index  $n = 1$ . However, in the disc we assume that the SFR takes place in two steps: first, molecular clouds form from the diffuse gas. Then stars form from cloud-cloud collision or by the interaction of the molecular clouds with massive stars. The first process in the halo depends on the volume with an efficiency taken as constant for all haloes. Conversely, the second process is a local one and also assumed to possess a constant efficiency. In our older MD05 models, we had assumed that the other two processes were dependent on the volume of the disk and on an efficiency considered to be a free parameter. Both of these latter efficiencies,  $\epsilon_c$  and  $\epsilon_s$ , for the cloud and star formation, respectively, were varied simultaneously through a number  $T$  which defined the set  $(\epsilon_c, \epsilon_s)$ . In this new grid of models we have included new prescriptions to form molecular gas from diffuse gas, thus eliminating the efficiency  $\epsilon_c$  as a free parameter. Finally only the efficiency  $\epsilon_s$  remains as a free parameter.

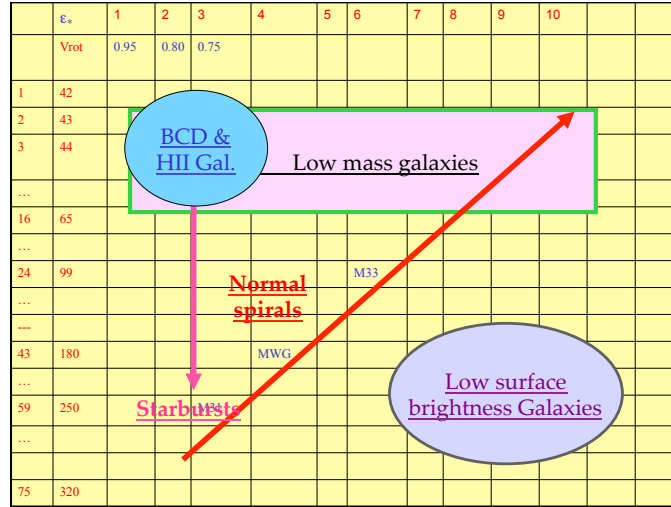


Figure 4: Scheme of our bi-parametric suite of models.

With these inputs we have finally a bi-parametric suite of models, as shown in Fig.4, defined by the virial mass (which implies the size of the disk and the collapse timescale) and the efficiency to form stars  $\epsilon_s$ . These models are valid for low mass galaxies as well as massive ones. The starburst or HII galaxies are included within the low mass and high efficiencies models, while low surface brightness galaxies will be among the more massive ones with low efficiencies. The MWG model corresponds to  $\log M_{\text{vir}} = 11.95$  and an efficiency  $\epsilon_s(T = 4)$ .

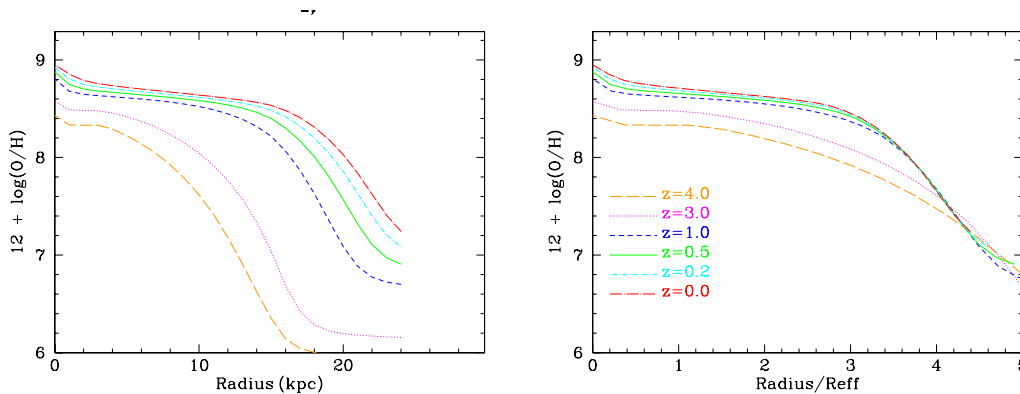


Figure 5: Radial distribution for the oxygen abundance,  $12+\log(O/H)$ , for 5 different redshifts:  $z=0, 0.5, 1, 2, 3$  and  $4$  with red, cyan, green, blue, magenta and orange lines, respectively, as a function of: left)  $R$  in  $kpc$ , and right) as a function of the normalized radius  $R/R_{\text{eff}}$ .

### 3 Results

One of the most important results derived from this work for our MWG model is the time evolution of the radial abundance gradient, in particular, for this work, oxygen. In Fig.5, left panel, we represent the oxygen radial distribution, as  $12 + \log(O/H)$  vs  $R$  for 5 different values of redshifts (see caption). The first thing we note is that it is impossible to distinguish the results among  $z = 0$  and  $z < 2$  when the radial range is restricted to  $R \sim 14$  kpc, that is around the optical radius or slightly larger. Only for higher redshifts is it possible to see a difference.

This implies that a clear separation in data coming from HII regions and PNe of 5-8 Gyr old will not be apparent, such as [40] find. The second fact we see here is that the radial gradient is the same for all redshift, when we measure it within the optical radius (which, obviously, decreases with increasing redshift). This way, for  $z = 4$  the radial gradient is the same as for  $z = 0$  when measured out only to  $R \sim 5$  kpc instead of (say) out to 15 kpc as in the case for redshift  $z=0$ . This is quite reasonable since beyond the optical radius there are few stars present to ionize the gas, and therefore deriving the gradient from the outer disk is not relevant for comparisons with empirical data. This fact is more clearly shown in the right panel of the same Fig.5, where  $12 + \log(O/H)$  is represented as a function of the normalized radius  $R/R_{\text{eff}}$ .

We have computed the temporal evolution of the radial oxygen gradient for the MWG model. To do so, we have fit a least-squares line to our results, restricting the fit to radii  $R < 3R_{\text{eff}}$ . The resulting evolution is shown by the blue line in Fig.6. In that figure we have also plotted some observational data from MWG [37, 54, 24, 60, 38, 21, 64, 12, 1], and also from the other spiral galaxies [65, 52, 27, 40]. We see that our new results for a MWG-like model are in better agreement with the most recent data, particular data derived from PNe. The predictions from cosmological simulations from [48] and [20] are also plotted, showing

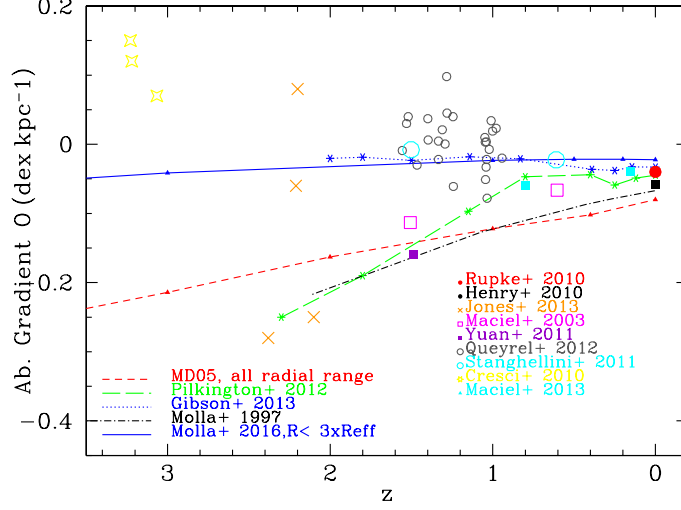


Figure 6: Radial gradient for the oxygen abundance, as  $\text{dex kpc}^{-1}$  as a function of redshift, compared with our old model predictions, with other data (see text), as labelled, and with cosmological simulations results from [48, 20].

that our new model also agrees with the last one in which the feedback of the star formation treatment is included. Much work remains to be done to explain the diversity of gradients beyond that of the MWG though; this is left to a more detailed future study.

## 4 Conclusions

1. A grid of chemical evolution models with 16 different total dynamical masses in the range  $10^{10}$  to  $10^{13} M_{\odot}$  is calculated.
2. 10 values of efficiencies  $\epsilon_s$  to form stars from molecular clouds are used ( $0 < \epsilon_s < 1$ ).
3. The best combination with an IMF from [31]+ stellar yields from [18, 19] + [35, 9], is used.
4. The stellar yields + IMF do not change the radial distributions of disks.
5. Using [58] prescriptions for  $M_{\text{halo}}/M_{\text{disk}}$ , we obtain the necessary infall rates to reproduce the radial profiles of galaxy disks
6. The HI-to-H<sub>2</sub> formation prescriptions from Ascasíbar & Romero (in prep.) seem the best ones to reproduce the MWG disk.
7. The slope of the Oxygen abundance radial gradient measured for  $R < 3R_{\text{eff}}$  has a value  $-0.06 \text{ dex kpc}^{-1}$ , or  $-0.12 \text{ dex } R_{\text{eff}}^{-1}$ , when measured versus a normalized radius,

in excellent agreement with the universal radial gradient obtained for CALIFA galaxies [57].

8. The same slope is obtained for all efficiencies and all galaxy masses.
9. This slope does not change much with redshift when the infall rate is as smooth as we have obtained recently, compared with old models with stronger evolution.

## Acknowledgments

This work has been supported by DGICYT grant AYA2013-47742-C4-4-P. This work has been supported financially by grant 2012/22236-3 from the São Paulo Research Foundation (FAPESP). This work has made use of the computing facilities of the Laboratory of Astroinformatics (IAG/USP, NAT/Unicsul), whose purchase was made possible by the Brazilian agency FAPESP (grant 2009/54006-4) and the INCT-A. MM thanks the kind hospitality and wonderful welcome of the Jeremiah Horrocks Institute at the University of Central Lancashire, the E.A. Milne Centre for Astrophysics at the University of Hull, and the Instituto de Astronomia, Geofísica e Ciências Atmosféricas in São Paulo (Brazil), where this work was partially done.

## References

- [1] Anders, F., Chiappini, C., Minchev, I., et al. 2016, A&A, submitted (arXiv:1608.04951)
- [2] Asplund, M., Grevesse, N., Sauval, A. J., & Scott, P. 2009, ARAA, 47, 481
- [3] Belley, J., & Roy, J.-R. 1992, ApJS, 78, 61
- [4] Blitz, L., & Rosolowsky, E. 2006, ARAA, 650, 933
- [5] Boissier, S., & Prantzos, N. 2000, *MNRAS*, 312, 398
- [6] Boissier, S., & Prantzos, N. 1999, A&A, 307, 857
- [7] Cavichia, O., Mollá, M., Costa, R. D. D., & Maciel, W. J. 2014, *MNRAS*, 437, 3688
- [8] Chiappini, C., Matteucci, F., & Gratton, R. 1997, ApJ, 477, 765
- [9] Chieffi A., Limongi M., 2004, ApJ, 608, 405
- [10] Clayton, D. D. 1987, ApJ, 315, 451
- [11] Cresci, G., Mannucci, F., Maiolino, R., et al. 2010, Nature, 467, 811
- [12] Cunha, K., Frinchaboy, P. M., Souto, D., et al. 2016, Astronomische Nachrichten, 337, 922
- [13] Diaz, A. I. 1989, Evolutionary Phenomena in Galaxies, 377
- [14] Diaz A. I., Tosi M., 1984, *MNRAS*, 208, 365
- [15] Ferrini F., Matteucci F., Pardi C., Penco U., 1992, ApJ, 387, 138
- [16] Ferrini F., Molla M., Pardi M. C., Diaz A. I., 1994, ApJ, 427, 745
- [17] Gallagher J. S., III, Hunter D. A., Tutukov A. V., 1984, ApJ, 284, 544
- [18] Gavilán, M., Buell, J. F., & Mollá, M. 2005, A&A, 432, 861

- [19] Gavilán M., Mollá M., Buell J. F., 2006, *A&A*, 450, 509
- [20] Gibson, B. K., Pilkington, K., Brook, C. B., Stinson, G. S., & Bailin, J. 2013, *A&A*, 554, A47
- [21] Genovali, K., Lemasle, B., Bono, G., et al. 2014, *A&A*, 566, A37
- [22] Goetz M., Koeppen J., 1992, *A&A*, 262, 455
- [23] Henry, R. B. C., & Worthey, G. 1999, *PASP*, 111, 919
- [24] Henry, R. B. C., Kwitter, K. B., Jaskot, A. E., et al. 2010, *ApJ*, 724, 748
- [25] Hou, J. L., Prantzos, N., & Boissier, S. 2000, *A&A*, 362, 921
- [26] Iwamoto, K., Brachwitz, F., Nomoto, K., et al. 1999, *ApJS* 125, 439
- [27] Jones, T., Ellis, R. S., Richard, J., & Jullo, E. 2013, *ApJ*, 765, 48
- [28] Karakas, A. I. 2010, *MNRAS*, 403, 1413
- [29] Kennicutt, R. C., Jr. 1998, *ApJ*, 498, 541
- [30] Koeppen J., 1994, *A&A*, 281, 26
- [31] Kroupa P., 2002, *Sci*, 295, 82
- [32] Kubryk M., Prantzos N., Athanassoula E., 2015, *A&A*, 580, A127
- [33] Lacey, C. G., & Fall, S. M. 1983, *MNRAS*, 204, 791
- [34] Lacey, C. G., & Fall, S. M. 1985, *ApJ*, 290, 154
- [35] Limongi M., Chieffi A., 2003, *ApJ*, 592, 404
- [36] Maciel W. J., Koppen J., 1994, *A&A*, 282, 436
- [37] Maciel, W. J., Costa, R. D. D., & Uchida, M. M. M. 2003, *A&A*, 397, 667
- [38] Maciel, W. J., & Costa, R. D. D. 2013, *RMxA&Ap*, 49, 333
- [39] Magrini L., Sestito P., Randich S., & Galli D. 2009, *A&A*, 494, 95
- [40] Magrini L., Coccato L., Stanghellini L., Casasola V., Galli D. 2016, *A&A*, 588, A91
- [41] Matteucci, F., & Francois, P. 1989, *MNRAS*, 239, 885
- [42] McCall, M. L., Rybski, P. M., & Shields, G. A. 1985, *ApJS*, 57, 1
- [43] Mollá M., Díaz A.I., Tosi M., 1990, in *Chemical and dynamical evolution of Galaxies*, eds. F. Ferrini, J. Franco, & F. Matteucci, ETS Editrice (PISA), 577
- [44] Mollá, M., Ferrini, F., & Diaz, A. I. 1997, *ApJ*, 475, 519
- [45] Mollá, M. & Díaz, A.I. 2005, *MNRAS*, 358, 521
- [46] Mollá, M., Cavichia, O., Gavilán, M., & Gibson, B. K. 2015, *MNRAS*, 451, 3693
- [47] Mollá, M., Díaz A. I., Gibson, B. K., et al., 2016, *MNRAS*,
- [48] Pilkington, K., Few, C. G., Gibson, B. K., et al. 2012, *A&A*, 540, A56
- [49] Portinari, L., & Chiosi, C. 2000, *A&A*, 355, 929
- [50] Prantzos, N., & Aubert, O. 1995, *A&A*, 302, 69
- [51] Prantzos, N., & Boissier, S. 2000, *MNRAS*, 313, 338

- [52] Queyrel, J., Contini, T., Kissler-Patig, M., et al. 2012, *A&A*, 539, A93
- [53] Ruiz-Lapuente P., Blinnikov S., Canal R., Mendez J., Sorokina E., Visco A., Walton N., 2000, *MmSAI*, 71, 435
- [54] Rupke, D. S. N., Kewley, L. J., & Chien, L.-H. 2010, *ApJ*, 723, 1255
- [55] Salucci P., Lapi A., Tonini C., Gentile G., Yegorova I., Klein U., 2007, *MNRAS*, 378, 41
- [56] Sancisi, R., Fraternali, F., Oosterloo, T., & van der Hulst, T. *A&ARv*, 15, 189
- [57] Sánchez, S. F., Rosales-Ortega, F. F., Iglesias-Páramo, J., et al. 2014, *A&A* 563, A49
- [58] Shankar F., Lapi A., Salucci P., De Zotti G., Danese L., 2006, *ApJ*, 643, 14
- [59] Shaver, P. A., McGee, R. X., Newton, L. M., Danks, A. C., & Pottasch, S. R. 1983, *MNRAS*, 204, 53
- [60] Stanghellini, L., & Haywood, M. 2010, *ApJ*, 714, 1096
- [61] Tinsley, B. M., & Larson, R. B. 1978, *ApJ*, 221, 554
- [62] Tosi, M., & Diaz, A. I. 1985, *MNRAS* 217, 571
- [63] Tosi M., 1996, in *From Stars to Galaxies: The Impact of Stellar Physics on Galaxy Evolution*, ASP Conference Series, eds. C. Leitherer, U. Fritze-von-Alvensleben, and J. Huchra, 98, 299
- [64] Xiang, M.-S., Liu, X.-W., Yuan, H.-B., et al. 2015, *Research in Astronomy and Astrophysics*, 15, 1209
- [65] Yuan, T.-T., Kewley, L. J., Swinbank, A. M., Richard, J., & Livermore, R. C. 2011, *ApJL*, 732, L14
- [66] Zaritsky, D., Kennicutt, R. C., Jr., & Huchra, J. P. 1994, *ApJ*, 420, 87